Geoacoustic inversion of transmission loss data

LEIF ABRAHAMSSON, BRODD LEIF ANDERSSON, STEFAN BAN,
EVA DALBERG, PER SÖDERBERG

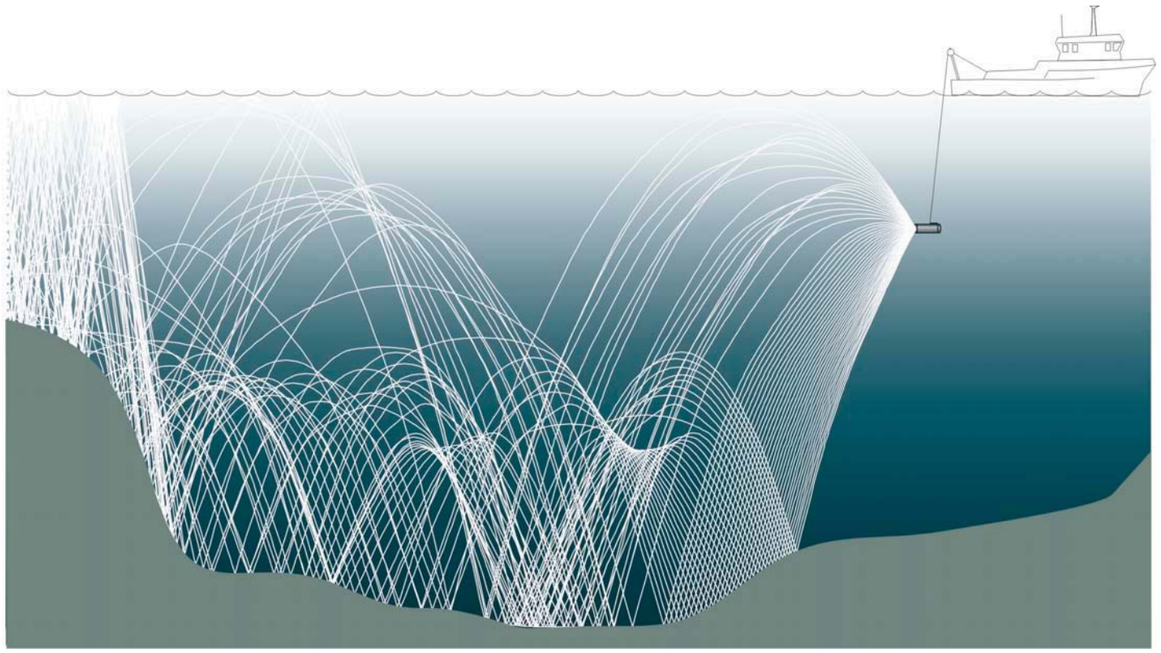

FOI is an assignment-based authority under the Ministry of Defence. The core activities are research, method and technology development, as well as studies for the use of defence and security. The organization employs around 1350 people of whom around 950 are researchers. This makes FOI the largest research institute in Sweden. FOI provides its customers with leading expertise in a large number of fields such as security-policy studies and analyses in defence and security, assessment of different types of threats, systems for control and management of crises, protection against and management of hazardous substances, IT-security an the potential of new sensors.

FOI
Defence Research Agency
Systems Technology
SE-164 90 Stockholm

Phone: +46 8 555 030 00
Fax: +46 8 555 031 00

www.foi.se

FOI-R-- 2020 --SE Technical report
ISSN 1650-1942 June 2006

Systems Technology

Leif Abrahamsson, Brodd Leif Andersson, Stefan Ban, Eva Dalberg, Per Söderberg

Geoacoustic inversion of transmission loss data

FOI-R--2020--SE
ISSN 1650-1942

Technical report
June 2006

Systems Technology

Issuing organization	Report number, ISRN	Report type
FOI – Swedish Defence Research Agency Systems Technology SE-164 90 Stockholm	FOI-R—2020--SE	Technical report
	Research area code 4. C4ISTAR	
	Month year June 2006	**Project no.** E60703
	Sub area code 43 Underwater Surveillance, Target acquistion and Reconnaissance	
	Sub area code 2	

Author/s (editor/s)	Project manager
Leif Abrahamsson Brodd Leif Andersson Stefan Ban Eva Dalberg Per Söderberg	Peter Krylstedt
	Approved by Monica Dahlén
	Sponsoring agency Swedish Armed Forces
	Scientifically and technically responsible Kurt Otto

Report title
Geoacoustic inversion of transmission loss data

Abstract

This report presents results of geoacoustic inversions based on broadband transmission loss data in the frequency range 0.1-4 kHz. The acoustic measurements were made in June 2005 in a coastal water area off Nynäshamn. High frequency signals were used to estimate the thickness of a low-speed surficial sediment layer. The inversion revealed that the thickness varied of the order 0-10 m both by range and azimuth. The bottom parameters of an underlying sediment were determined by inversion of low frequency data. Also this sediment showed varying characteristics along different measurement tracks.

In the inversion, bottom parameters are searched that give a best fit of measured and simulated sound fields (the matched-field technique). Two sound propagation models, one based on ray tracing and the other one on the parabolic wave equation, were used.

Comparisons between this experiment and a previous inversion study of reflection loss data from the same site are presented with respect to inversion results and their importance to operational rapid environment asssessment (REA). Guidelines for future work on inversion techniques based on mobile data acquisition systems are proposed.

Keywords
underwater acoustics, inversion, transmission loss, matched-field

Further bibliographic information	Language English

ISSN 1650-1942	Pages 24 p.
	Price acc. to pricelist

Utgivare FOI - Totalförsvarets forskningsinstitut Systemteknik 164 90 Stockholm	**Rapportnummer, ISRN** FOI-R--2020--SE	**Klassificering** Teknisk rapport
	Forskningsområde 4. Ledning, informationsteknik och sensorer	
	Månad, år Juni 2006	**Projektnummer** E60703
	Delområde 43 Undervattenssensorer	
	Delområde 2	

Författare/redaktör Leif Abrahamsson Brodd Leif Andersson Stefan Ban Eva Dalberg Per Söderberg	**Projektledare** Peter Krylstedt
	Godkänd av Monica Dahlén
	Uppdragsgivare/kundbeteckning Försvarsmakten
	Tekniskt och/eller vetenskapligt ansvarig Kurt Otto

Rapportens titel

Geoakustisk inversion av transmissionsförlustdata

Sammanfattning

I denna rapport redovisas geoakustiska inversionsresultat baserade på bredbandiga transmissionsförlust-data i frekvensområdet 0.1-4 kHz. De akustiska mätningarna utfördes i juni 2005 i ett kustnära försöks-område utanför Nynäshamn. Högfrekventa signaler användes för att uppskatta tjockleken av ett mjukt ytsediment med lägre ljudhastighet än den i vattnet. Inversionen visade på variationer i tjocklek av storleksordningen 0-10 m i både avstånd och riktning. Bottenparametrar för ett underlagrat sediment bestämdes med inversion av lågfrekventa data. Också detta sediment uppvisade varierande egenskaper längs de olika mätlöporna.

I inversionsmetoden söker man bottenparametrar som ger en bästa anpassning mellan uppmätta och simulerade ljudfält (matched-field tekniken). Två ljudutbredningsmodeller, en baserad på strålgång och den andra på den paraboliska vågekvationen, användes.

Jämförelser mellan detta experiment och ett tidigare inversionsförsök med reflektionsdata från samma mätplats presenteras med avseende på resultat och deras betydelse för operationella REA tekniker. Riktlinjer för det fortsatta arbetet med inversion baserad på mobila datainsamlingssystem föreslås.

Nyckelord

undervattensakustik, inversion, transmissionsförlust, matched-field

Övriga bibliografiska uppgifter	**Språk** Engelska
ISSN 1650-1942	**Antal sidor:** 24 s.
Distribution enligt missiv	**Pris: Enligt prislista**

Contents

1 Introduction

Modern tactical aid systems for naval operations are equipped with increasingly sophisticated tools where accurate knowledge of the underwater environment is essential in order to reach full performance of the systems. Besides the sound speed and water depth, the acoustic properties of the seabed are the most important environmental parameters. The geoacoustic parameters of the seabed must be determined indirectly by interpretation of measured sound pressure levels in the water. Research at FOI aims at developing fast techniques to determine such parameters under operational conditions. This capability is specifically important during missions in foreign areas where the amount and quality of sediment data is limited.

The purpose of this paper is to report geoacoustic inversion results based on acoustic measurements in June 2005 in a coastal water area off Nynäshamn. Six different broadband waveforms (chirps) spanning a frequency range of 0.1-4 kHz were transmitted from a towed source. The signals, propagated over distances of 0.25-4 km, were received by a bottom-moored vertical array. High frequency data were used to invert for surficial sediment parameters, while those of an underlying sediment were determined by inversion of low frequency data. A matched-field inversion technique was applied. It means that the bottom parameters are determined by minimizing a fitness function, which quantifies the mismatch between the measured and simulated sound fields. While the high-frequency inversions of the upper sediment layer were carried out by a fast ray trace solver, the low-frequency inversions of the lower sediment required a computationally more demanding parabolic equation (PE) model. To gain computational speed, the PE-model was implemented to run on a cluster of PC-nodes.

Geoacoustic inversion results for two different tracks are reported. It was found that the bottom properties vary both by depth and range in different ways along the two tracks. The inversion of high frequency data revealed the presence of a low-speed surficial sediment layer at the deep parts of the tracks. Beneath the top layer a sandy sediment with high velocity and density was identified by inversion of low frequency data. As opposed to the top layer, the thickness of the hard sediment is larger at the shallow parts of the tracks than at the deep ones. It was observed that effects of shear wave excitation in the lower sediment must not be neglected for signals below 250 Hz.

Acoustic data at an intermediate frequency band around 500 Hz were mostly used for validation of inversion results obtained from data at complementary frequencies. Additional consistency checks of the estimated bottom parameters were provided by wave propagation modeling of ship noise from the vessel that towed the sound projector. The tests confirmed that fair predictions could be made by running sound propagation models with the estimated bottom parameters as part of the environmental input.

This paper is organized as follows. Section 2 is a description of the field trial and the characteristics of collected data. Section 3 contains a model analysis of the high signal losses suffered at propagation at downward refraction in conjunction with a low-speed surficial sediment. The building blocks of the inversion scheme and the inversion results with validations are presented in Secs. 4 and 5. Section 6 is a summary of key points of importance for operational rapid environment assessment (REA).

2 The field measurements

This work is a follow up of the inversion of reflection loss measurements reported in [1]. An account of the geology of the test area, and further details of the data acquisition system, is found in that reference.

2.1 Experimental description

The sonar measurements were made on June 13 2005 in a coastal water area near Nynäshamn. The site of the vertical receiver array was the same as for the reflection loss measurements, which took place two weeks earlier [1]. In the intervening period, while the array was kept bottom-moored in the sea, the integrity of the topmost 7 elements was lost. Therefore transmission loss data were received on the remaining 24 elements, which spanned water depths from 14 to 24.5 m. The water depth at the location of the array was around 25 m. The research vessel HMS Ägir was employed for transmissions along radial tracks in the NW, SW and S directions with the array at the center. Broadband pulses were transmitted at nominal distances 0.25, 0.5, 1, 2, and 4 km. Once the ship was positioned at the nominal range, the engines were turned off and signals were emitted at a source depth of 15 m. The GPS coordinates of the drifting ship were recorded simultaneously with the transmissions. The drift motion of the ship during the transmission time was at most 100 m. The wind speed was 3–4 m/s.

A typical sound speed profile taken at the time of the acoustic measurements is shown in Fig. 2.1. The decreasing sound speed by depth will result in downward refraction of sound waves as illustrated by the accompanying ray diagram.

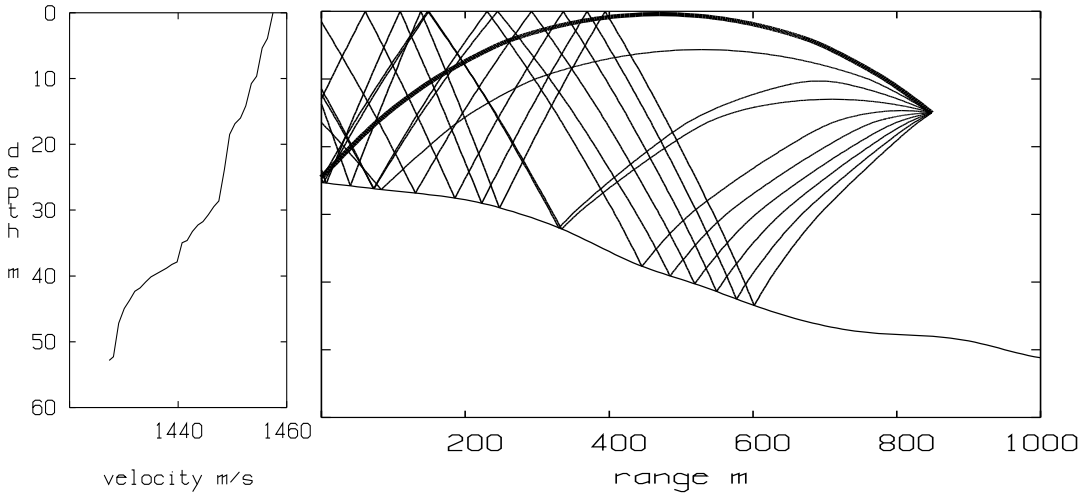

Figure 2.1: *Left: The measured sound speed profile at the test site on June 13, 2005. Right: The fan of ray traces launched in a ±4° angular sector at a range of 850 m illustrates the downward refraction of the sound field. The bold ray is a limiting ray, which shows that there is no direct source-receiver paths at ranges beyond 850 m.*

The bathymetry along the tracks is shown in Fig. 2.2.

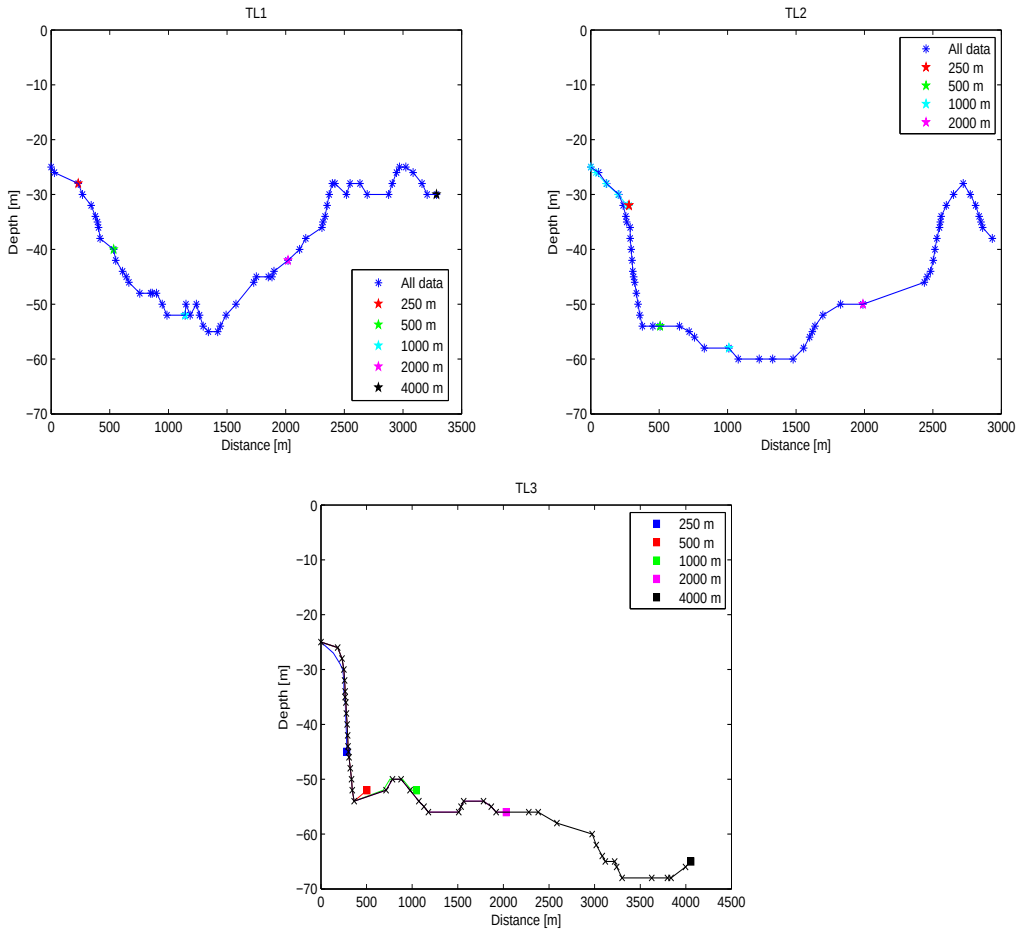

Figure 2.2: *The bathymetry along the tracks, designated TL1, TL2 and TL3, which were in the NW, SW and S directions from the array. The range is measured from the site of the array. Color- labeled stars indicate the source positions along the tracks.*

The three-dimensional character of the topography is obvious. The bathymetry around the array is gently downsloping out to a range of 250 m, where the water depth increases by a factor of two in a short distance. The change of water depth around 250 m is most pronounced along track 3.

2.2 Acoustic data

Provisions were made to ensure proper calibration of received signals. A reference hydrophone was positioned in front of the transmitter, from which the following source levels [dB re 1 μPa] at 1 m were obtained:

125 Hz: 165.9, 250 Hz: 166.9, 500 Hz: 166.7

1 kHz: 166.7, 2 kHz: 167.9, 4 kHz: 161.5

Two of the hydrophones were calibrated in a tank laboratory before the trial. The sensitivity of the remaining ones were determined *in situ* using transmissions at short ranges (25–60 m) from the array.

The transmit signals were Ricker chirps [1] with center frequencies at 0.125, 0.25, 0.5, 1, 2, and 4 kHz with bandwidths of the same order as the center frequency. The corresponding pulse lenghts were 480, 240, 120, 60, 30, and 15 ms. The six signals were transmitted in a sequence separated by a time interval of 5 s. About 6–10 contiguous sequences were transmitted at each source-receiver offset. One of the pings at each nominal range and each frequency was selected for inversion. The recorded signals were crosscorrelated with the synthetic waveform being fed to the signal generator of the transmission unit. The correlated output was normalized by the energy integral of the source pulse, which preserves the signal amplitude while noise is suppressed. The improvement of the signal-to-noise ratio (SNR) amounts to $10 \log BT$ [dB], where BT is the time-bandwidth product. Using effective values of B and T of the Ricker chirps, the expected gain is 16 dB.

The sound intensity ($|p|^2$) was evaluated after matched filtering using the envelope squared of the analytic signal, that is,

$$\begin{aligned} |p(t)|^2 = &\quad p_r^2(t) + p_i^2(t) \\ p_r(t) = &\quad \text{matched filtered time series} \\ p_i(t) = &\quad \text{Hilbert transform of } p_r. \end{aligned}$$

Finally, the average of the envelope squared over all hydrophones was formed. This time series, expressed in dB, constitutes the main descriptor of data being used for inversion. Samples of such time series are shown in Fig. 2.3.

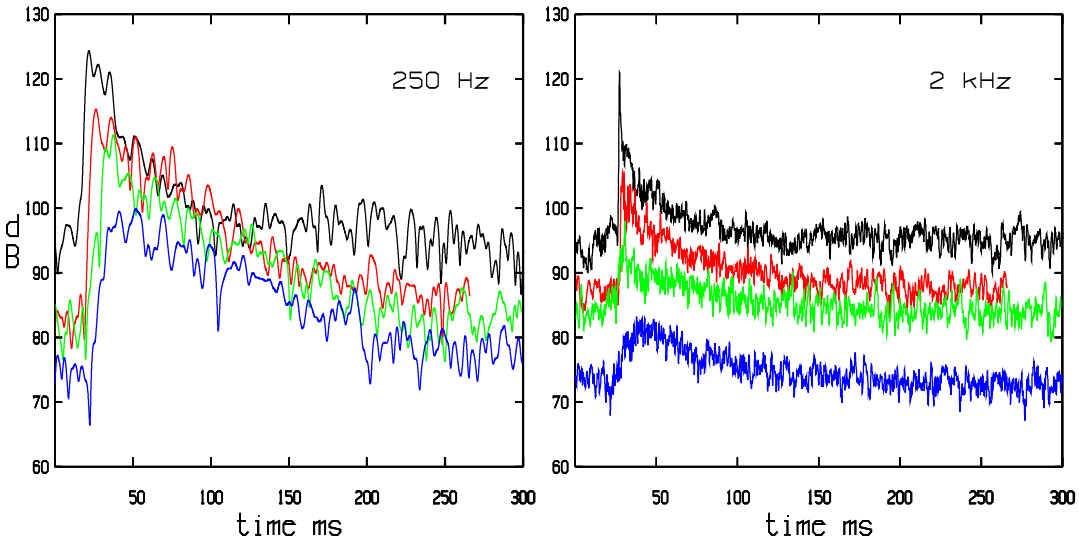

Figure 2.3: *Depth averaged intensities in dB versus time of broadband pulses centered at 250 Hz (left) and 2 kHz (right) at source ranges of 0.25 (black), 0.5 (red), 1 (green) and 2 km (blue). The signals have been displaced along the time axis so that the arrival times are about the same.*

The initial arrival has a sharp front after which the signal decays in a period of time

that is much longer than the duration of the emitted pulse. The intensity falls off faster at higher frequencies.

The background signal seen both prior to the first arrival and at the tail is caused by auxiliary machinery on HMS Ägir. Its source level was estimated by extrapolation from the observed field at the range 250 m to an acoustic center near the sea surface. It resulted in the following estimates [dB re 1 μPa]:

125 Hz: 134.0, 250 Hz: 133.6, 500 Hz: 142.7

1 kHz: 144.2, 2 kHz: 143.2, 4 kHz: 132.2

Fig. 2.4 shows transmission loss along all tracks at the nominal ranges 0.25, 0.5, 1, and 2 km.

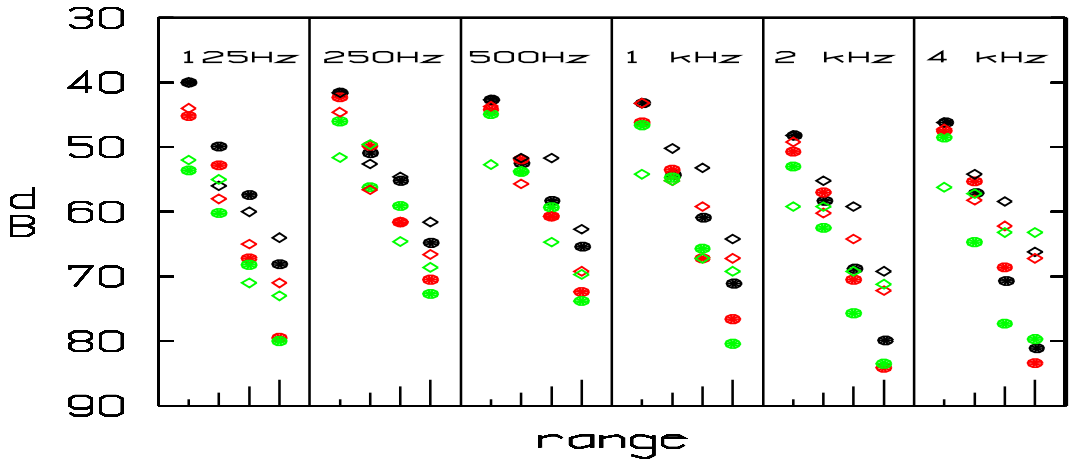

Figure 2.4: *Transmission loss as function of range at the nominal ranges 0.25, 0.5, 1, and 2 km along track 1 (black), track 2 (red), and track 3 (green). These ranges are represented by tick marks of increasing lengths at the bottom of each frequency panel. The transmitted signals are marked by solid circles, while the open squares denote the ship noise from HMS Ägir.*

The loss estimates of the broadband pulses refer to peak values of the depth averaged intensity, while those of the background signal were obtained by both depth and time averaging. The background source sends continuously and the received signal is built up to higher levels by multipath contributions as opposed to the transient signals which are dispersed in time proportionally to the source-receiver range. This might explain the large differences of loss seen at the longer ranges. Irrespective of the way loss is measured, the high losses as the propagation range increases from 1 to 2 km are noteworthy. The increase is in most cases larger than the spherical rate of decay of 6 dB. In conjunction with the observation that the loss at 1 km is around 60 dB it means that the overall loss beyond 1 km is in parity with, or for the high frequencies even larger than the spherical spreading loss. In comparing the levels along track 1 and track 2, we see that the loss is larger along track 2, in particular at low frequencies. The loss figures along track 3 exhibit some anomalies. For example the loss of the 125 Hz pulse is exceptionally large and the high frequency pulses suffer huge losses in the

range 0.5–1 km. As there is some evidence of data uncertainty, the data sets of track 3 have been excluded from the inversion.

Fig. 2.5 illustrates the vertical directionality versus time of the 1 kHz pulse at the ranges 0.25 and 1 km along track 1.

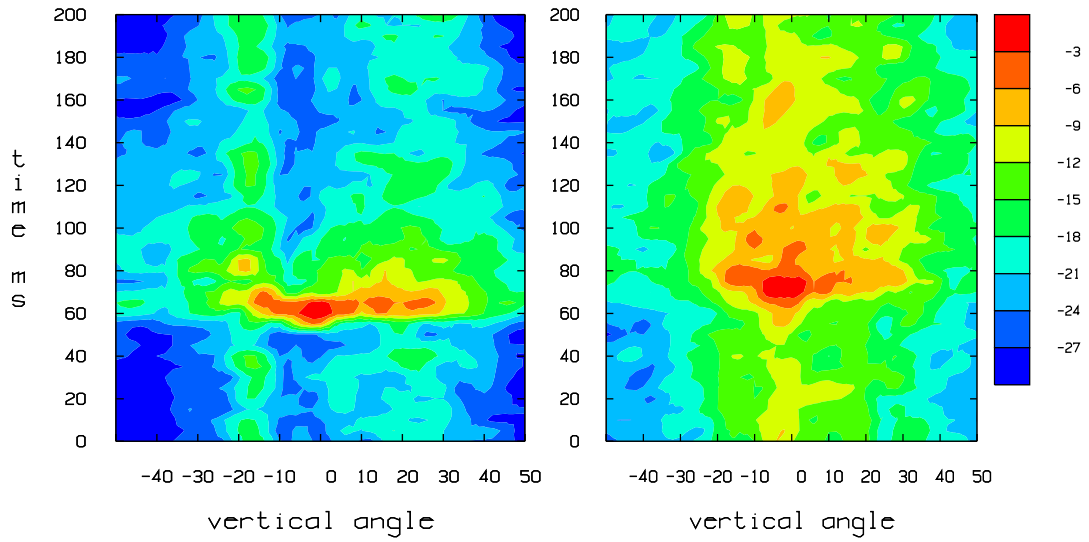

Figure 2.5: *Vertical directionality as a function of time of the 1 kHz pulse at 0.25 (left) and 1 km (right) along track 1. The signals have been displaced along the time axis so that the arrival times are about 60 ms in the above time window. Angles (degrees) are measured with respect to the horizontal with negative values for arrivals from the sea surface. The scale (dB) is normalized with respect to the peak amplitude at each range.*

We see that the angular spread is essentially confined to a sector within $\pm 30^{\circ}$. We also note that the duration of the pulse is shorter at the closer source range (left picture). The background of ship noise is clearly seen both before and after the arrival of the transmitted pulse. A notable feature is the notch around the horizontal direction at the short range 250 m, which is absent at the source range 1 km. Similar patterns are frequently observed in measurements of ship- and wind-generated noise [2].

The filtering effect on a recording of ambient noise is illustrated in Fig. 2.6. The average intensity level of the time-series of noise before filtering was 94 dB. The corresponding levels of the matched filtered noise were 67, 72, 75, 76, 73, and 68 dB as the center frequency of the chirps ranged from 0.125 to 4 kHz. The standard deviation amounted to 4 dB in all cases. Although these levels are not significantly high, the signals being sent from 4 km along tracks 2 and 3 were not discernible. Along track 1, where the maximum range was limited to 3.3 km due to shoaling, the reception was weak.

Taken together a persistent feature of field data is the large decrease of SNR at ranges beyond some kilometres. Such high losses have also been observed from measurements in the Stockholm archipelago [3],[4].

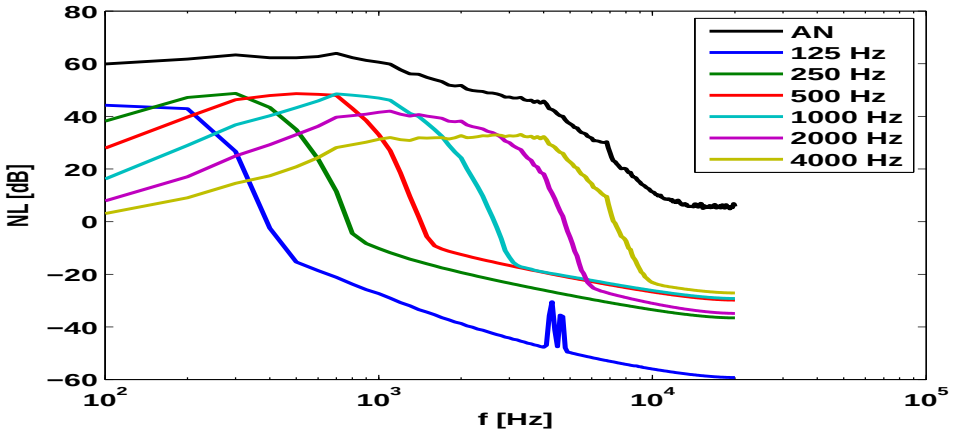

Figure 2.6: *The spectral noise level* [dB re 1 μPa/$\sqrt{\text{Hz}}$] *of a 10-s noise recording at the time of the experiment. The corresponding levels after matched filtering by the transmit pulses are shown in color and labeled by the center frequency of the pulse.*

3 Modeling aspects

A plausible cause of the large losses exhibited by data is the presence of a soft surficial sediment. The effect of a thin and soft bottom layer was studied in [5, 6]. In this section, the additional influence of the sound speed of the water column is taken into account. It will be shown that the combined effect of a downward refracting sound speed profile, and a soft bottom with a thickness of a few wavelenghts, may incur high losses.

3.1 A nominal geoacoustic model

For the analysis, and later for the geoacoustic inversion, we consider a geoacoustic model consisting of three bottom layers:

$$\begin{array}{lllllll} \text{layer 1:} & c_{p1}=1400, & \rho_1=1.2, & \beta_{p1}=0.15, & h_1=5 & & \\ \text{layer 2:} & c_{p2}=1650, & c_{s2}=388 & \rho_3=1.77, & \beta_{p2}=1.1, & \beta_{s2}=0.7, & h_2=20 \\ \text{layer 3:} & c_{p3}=5200, & c_{s3}=3000, & \rho_3=2.6, & \beta_{p3}=0.2, & \beta_{s3}=0.3 & \end{array} \tag{3.1}$$

with the notations

$$\begin{array}{rl} c_p/c_s: & \text{compressional/shear velocity} \quad [\text{m/s}] \\ \beta_p/\beta_s: & \text{compressional/shear absorption} \quad [\text{dB}/\lambda] \\ \rho: & \text{density} \quad [\text{g/cm}^3] \\ h: & \text{layer thickness} \quad [\text{m}] \end{array}$$

This model has a low-speed uppermost layer with fluid-like properties. This feature is often encountered in both shallow and deep seas [6, 7, 8, 9, 10, 11]. Its parameters

are set according to the results of the geoacoustic inversions [12, 13]. The attenuation 0.15 dB/λ] is presumably larger than the intrinsic absorption, and it could be regarded as an effective parameter, which also includes scatterring losses due to irregular embeddings of sand. Sediment coring analyses [14, 15, 16] often show that the top layer is heterogeneous on a scale less than 1 m. The geoacoustic parameters of the intermediate layer correspond to fine sand for which rigidity and absorption are relatively large [17]. The deepest layer is a basement of granite, which is assumed to have a semi-infinite extent in depth.

3.2 Reflection loss features

A primary characteristic of the acoustic response of the bottom is given by the reflection coefficient R, or the reflection loss $-20log|R|$, of a plane wave incident from an overlying and homogeneous water column. In a layered medium, reflection loss depends on the frequency. A hard bottom covered by a thin and soft layer may exhibit bottom loss anomalies at certain frequencies ususally related to a layer thickness of the order of a quarter of a wavelength [5]. The occurrence of high losses shows up as sharp peaks in graphs of loss curves versus frequency, grazing angle or layer thickness. In the following analysis such effects are smeared out by averaging over both frequency and layer thickness. One reason for applying averaging is that the inversions in this study are based on broadband signals. Another one is concerns about the presence of distinct frequency features in real sea environments, where the horizontal stratification may be imperfect.

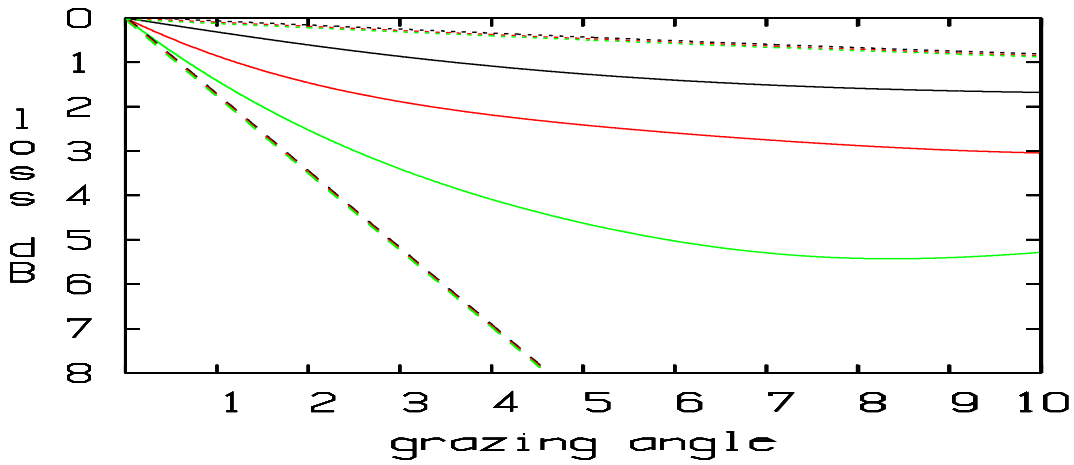

Figure 3.1: *Average reflection loss versus grazing angle (degrees) for the frequency bands* $[90, 100]$ *(black),* $[450, 550]$ *(red) and* $[900, 1100]$ *Hz (green) with additional averaging over the thickness parameter* h_1 *in the range* $[3, 7]$ *m. The reference cases* $h_1 = 0$ *(dotted curves) and* $h_1 = \infty$ *(dashed curves) are coincident w r t frequency.*

Fig. 3.1 shows reflection loss as a function of grazing angles between 0° and 10° for an average taken over the thickness of the top layer $[3, 7]$ m and additionally over the frequency bands $90, 110$, $[450, 550]$ and $[900, 1100]$ Hz. As a reference the reflection losses for the limiting cases $h_1 = 0$ (no soft layer) and $h_1 = \infty$ (semi-inifinte soft layer) are also displayed. The reflection coefficient of the latter case is entirely frequency

independent, while this is almost true in the former case at the current frequencies. The velocity of the water column was set to 1430 m/s. It implies that most energy is injected into the low-velocity top layer with little backreflection at the water-bottom interface. The local reflection properties of this surface is represented by the $h_1 = \infty$ curve. The intermediate sediment is a strong reflector for waves with grazing angles below the critical angle

$$\cos^{-1} \frac{c_{p0}}{c_{p2}} = \cos^{-1} \frac{1430}{1650} \approx 30^\circ.$$

The loss at reflections below the critical angle is caused by the absorption parameters of the hard sediment and excitation of shear waves, which propagate to larger depths. We note that there is a huge difference between the limiting cases of an infinite soft layer and the absence of such a layer except for very near grazing incidence. We also see that the impact of the soft layer is substantial despite its thickness is merely of the order 3–7 m. The absorption loss when the wave traverses this layer increases by the frequency, and shallow angles are more lossy because of elongated path lengths through the top layer. However, in the very vicinity of grazing the loss is small as the reflection coefficient $R \approx -1$ for any kind of bottom that provides an impedance contrast.

3.3 Transmission loss features

The reflection loss describes the loss of a single bounce at the bottom. In shallow water, sound will propagate outwards from the source by repeated reflections between the water surface and the bottom (in the absence of internal sound channels). For a water depth of H m, and a constant sound speed, sound waves will undergo a bottom reflection at each range increment (cycle distance) of $2H/\tan\theta$ m, where θ is the ray angle relative to the horizontal plane (grazing angle). For a downward refracting sound speed profile, the cycle distance decreases as compared with the isovelocity case, especially for small grazing angles. In addition the angle of propagation steepens as the wave travels towards the bottom, which in turn precludes the low reflection loss area in the immediate vicinity of grazing. Altogether this implies that both the number of bottom bounces, and the reflection loss at each bounce, increase in the case of a downbending sound speed profile.

Fig. 3.2 shows transmission loss at a source-receiver range of 5 km both for the case of an isovelocity water column and for the downbending sound speed profile in Fig. 2.1 versus the velocity c_{p1} of the top layer, as it is varied in the range $[1400, 1650]$ m/s. The density and the absorption of the top layer are also increased linearly so that these values assume the corresponding values of the hard sediment at the end of the velocity range. The water depth is set to 50 m and the source depth to 15 m. The sound intensity has been averaged over frequency bands, depth points spanning the water column, and as the thickness of the top layer is varied between 3 and 7 m. The computations were performed by the normal-mode propagation model MODELOSS [18].

The most obvious feature is the wide span between low and high losses, which amounts to tens of dB. Compared with the spherical spreading loss of 74 dB for a source range of 5 km, the loss is anomalously large at 0.5 and 1 kHz for a low-velocity top layer in

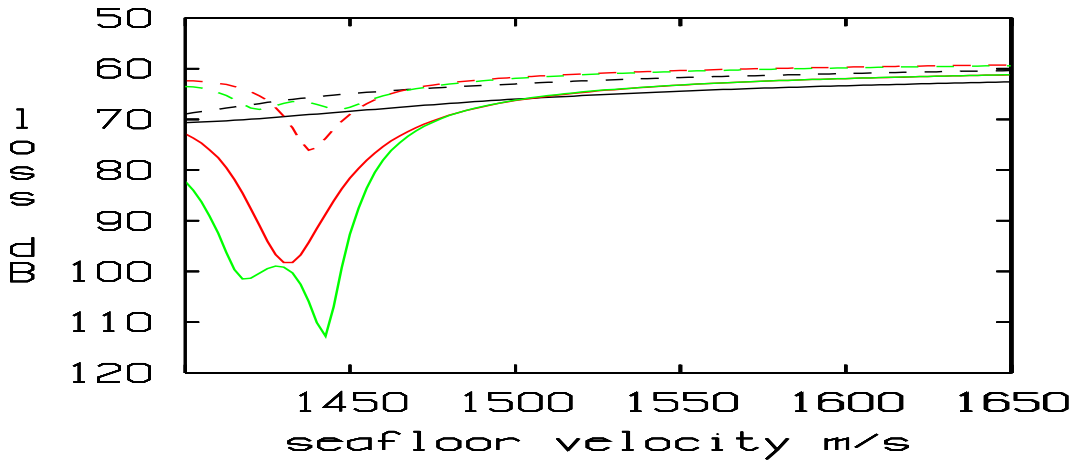

Figure 3.2: *Transmission loss at 5 km versus the velocity of the surficial sediment for the frequency bands* $[90, 110]$ *(black),* $[450, 550]$ *(red) and* $[900, 1100]$ *Hz (green) with additional averaging over depth points and the thickness parameter* h_1 *in the range* $[3, 7]$ *m. The dashed curves show transmission loss for an isovelocity water column (1450 m/s), while the solid curves are those for the velocity profile in Fig. 2.1.*

the case of downward refraction of sound in the water column. The reason is that the least grazing angle that can be achieved with the current water depth, source position and the sound velocity profile is about 10°. From the reflection diagram in Fig. 3.1, we see that the loss per bounce at 1 kHz and 10° amounts to 5 dB. The cycle distance of a ray launched horizontally at the source depth is 866 m. At a range of 5 km it implies that the total reflection loss is roughly 25 dB.

When the velocity of the uppermost sediment exceeds the water velocity by some 50 m/s, then the influence of the sound speed profile is not critical, although differences of 5 dB are noticable. We see that the loss diminishes for higher velocity bottoms, but even for a bottom velocity as low as 1500 m/s the loss at 5 km is 8 dB less than the spherical spreading loss of 74 dB.

4 Matched-field geoacoustic inversion

4.1 Objective function

Matched-field inversion techniques are applied to estimate bottom parameters. The basic principle is to find a best fit between measured data and sound fields computed by an acoustic propagation model which is driven by a parameterized seabed and the same probing source pulses as being used in the experiment. In the present study, the data/model mismatch is evaluated by the fitness function

$$F(s) = \min_{|m| \le M, |a| \le A} \left(\frac{1}{N} \sum_{n=1}^{N} (R_n^{dat} - R_{n-m}^{mod}(s) - a)^2 \right)^{\frac{1}{2}}, \quad [\text{dB}] \tag{4.1}$$

where

$$
\begin{aligned}
\mathrm{N} &= \text{number of time samples in the data window} \\
R_n^{dat} &= \text{measured intensity in dB at the nth time sample} \\
R_{n-m}^{mod}(s) &= \text{computed intensity in dB at the (n-m)th time sample} \\
s &= \text{search space of bottom parameters} \\
a &= \text{correction factor to account for uncertainty of source level} \\
m &= \text{delay index to correct for uncertainty of source-receiver distance}
\end{aligned}
$$

The time series R_n^{dat} and R_n^{mod} are the mean of the intensity across the 24 elements of the vertical array. As the sampling rate of field and model data need not be the same, the depth averaged intensities were linearly interpolated at common time points spaced by 0.05 ms. The time series were also smoothed by time averaging within a sliding window of the width 5 ms. The data window selected for the inversion comprises the elapsed time from the initial arrival until the intensity has fallen to some 10 dB above the background noise level.

The evaluation of the fitness function (4.1) involves a local optimization problem to account for uncertainties of the measurements of the source-receiver range and the intensity. The upper bound M of the delay index was constrained so that it corresponded to a range window of ± 20 m for allowable adjustments of the source range. The uncertainty interval A of the source level was restricted to stay within ± 1 dB.

4.2 Seabed parameterizations

The minimization of $F(s)$ is done over a search space s of bottom parameters of the geoacoustic model (3.1). This model comprises 13 geoacoustic parameters and two layer thicknesses that may vary by range. The parameters of the crystalline bedrock are assumed to be known and held fixed at the nominal values in (3.1). Further reductions of the dimension of the search space can be obtained using empirical relationships between geoacoustic variables. There are regression formulas or look-up tables by which the density [19], the compressional absorption coefficient [20], and the shear velocity/absorption [21] can be estimated in terms of the compressional wave velocity. If they are applied to the present model there remain four parameters, the compressional velocities and the thicknesses of the two sediments.

4.3 Propagation models

The frequency band of the field data extends from some 50 Hz to 5 kHz. The transmission ranges vary from 250 m to 2 km spanning water depths between 25 and 70 m. The three-layered bottom model are assumed to consist of a fluid layer on top of a shear supporting sediment and a solid basement. The thicknesses of the sediments may vary by range. The wide variety of frequency, geometry, and bottom structure require several modeling tools. For the inversion of range-dependent cases, the parabolic equation model was applied in the low frequency regime ($\lesssim 500$ Hz). The computations were performed by the program JEPE-S [22]. At higher frequencies the ray tracing program RAYLAB [23] was used.

The basic output of these codes is a complex number at each field point, which represents the amplitude of the sound field from a time-harmonic point source. Sound fields from broadband sources are synthesized by time-harmonic solutions using Fourier techniques. The number of frequencies required for the synthesis depends on the bandwidth of the source and the demand on frequency resolution. In the present experiment, source excitation was provided by Ricker chirps [12], whose autocorrelation is a Ricker pulse. The source function can be convolved by the transfer and filtering operators in any order of a time-invariant propagation model. In the present case, it implies that matched filtered data can be simulated by model calculations driven by Ricker pulses. It has the computational advantage that the frequency representation of a Ricker pulse is sparser than the corresponding chirp. Besides the frequency content of the source function, the frequency resolution is constrained by the inverse of the duration of the signal at the receiver.

The simulations of the propagation of ship noise were accomplished by using a point source at the depth 2 m. The source function was generated by a stochastic time-series of normally distributed pseudo-random numbers, which was filtered according to the measured spectral density distribution of ship noise. The frequency resolution was defined by the desired time window of the output at the receiver.

In order to check the consistency of the computational models, comparisons were made on a selection of propagation problems for which the assumptions of the derivations of the models were satisfied. The observed disagreements in terms of the fitness function (4.1) were mostly within 1 dB.

5 Inversion results

The inversion was partitioned into a sequence of subproblems in which shallow bottom parameters were determined prior to deep ones. Similarly the range interval was divided into segments which were processed step-by-step by marching in range and making use of inversion results at shorter source-receiver ranges.

5.1 The upper sediment

The inversion of high frequency data was limited to two bottom parameters, the thickness (h_1) of the upper sediment and the compressional velocity (c_{p2}) of the lower sediment. The remaining parameters of the upper sediment were held fixed according to the nominal model (3.1). The remaining parameters of the lower sediment were allowed to vary, but constrained by empirically based regression formulas in terms of the compressional velocity. Range-dependence of the target parameters was introduced at breakpoints at 0.25, 0.5, 1, and 2 km, that is at the source-receiver distances. The parameters were assumed to be piecewise constants between breakpoints except for a smooth transition region. The inversion proceeded from shorter to longer ranges and obtained results were inserted as they became available. The two-parameter inversion at each range was performed by an exhaustive search over thicknesses (h_1) between 0–24 m and velocities (c_{p2}) between 1500–1900 m/s. The search was made on a uniform grid with a thickness and velocity resolution of 0.6 m and 25 m/s. Forward modeling

was provided by ray tracing using eigenrays. The computation of the eigenrays need to be done once for each source and hydrophone position as the eigenrays are common for all frequencies and for any choice of bottom parameters.

Separate inversions were done for each frequency and at each range. The results obtained at a specific frequency were checked for consistency at other frequencies. A selection of results were made with preference for results that exhibited a high sensitivity as the target parameters were varied. Tables 5.1 and 5.2 show both inversion results and consistency checks in terms of the fitness function. The inversions along track 1 at the source ranges 500 m and 1 km, and along track 2, source range 500 m, were inconclusive and discarded. Instead the inversion results obtained at 250 m were extended to hold over these ranges. The fitnesses of this extrapolation were almost as good as the ones from the inversions at these ranges. The uncertainty of the inversion between 250 and 500 m will affect the inversions at the larger ranges and degrade the reliability. For this reason, particular attention must be paid to consistency checks.

	Range 250 m				Range 1 km				Range 2 km			
frequency [kHz]	0.5	1	2	**4**	0.5	1	2	4	0.5	**1**	2	4
fitness [dB]	1.9	1.4	2.7	**1.2**	3.3	3.2	3.4	3.2	3.1	**3.0**	2.8	2.8
h_1 [m]	0.7				0.7				3.7			
c_{p2} [m/s]	1725				1725				1900			

Table 5.1: *Track 1 model/data fitness values of the inversion for the inverted parameters h_1 and c_{p2} of the geoacoustic model (3.1). The frequency and fitness of the data set selected for inversion are typed in boldface, while fitness values at other frequencies were evaluated using the inversion results of those marked by boldface.*

	Range 250 m				Range 1 km				Range 2 km			
frequency [kHz]	0.5	1	2	**4**	0.5	1	**2**	4	0.5	1	**2**	4
fitness [dB]	1.9	1.4	1.8	**1.7**	2.5	1.6	**1.6**	2.8	4.6	1.9	**2.3**	1.1
h_1 [m]	0.7				9.7				7.9			
c_{p2} [m/s]	1725				1600				1650			

Table 5.2: *Track 2 model/data fitness values of the inversion for the inverted parameters h_1 and c_{p2} of the geoacoustic model (3.1). The frequency and fitness of the data set selected for inversion are typed in boldface, while fitness values at other frequencies were evaluated using the inversion results of those marked by boldface.*

The inversion results reveal that the thickness of the upper sediment is thin at short ranges while it becomes sizable in the range of 1–2 km. The thickness and rate of growth is larger along track 2. The speed estimates indicate that the lower sediment is hard.

Ambiguity plots are helpful to gauge the uncertainty of these estimates. Such a plot is shown in Fig. 5.1 for the inversion of 4 kHz data at the propagation range 250 m along track 1.

As indicated by the color bar, the dynamic range in dB varies between 1 and 10 dB. This plot shows that the ambiguity of the thickness estimate amounts to a few metres.

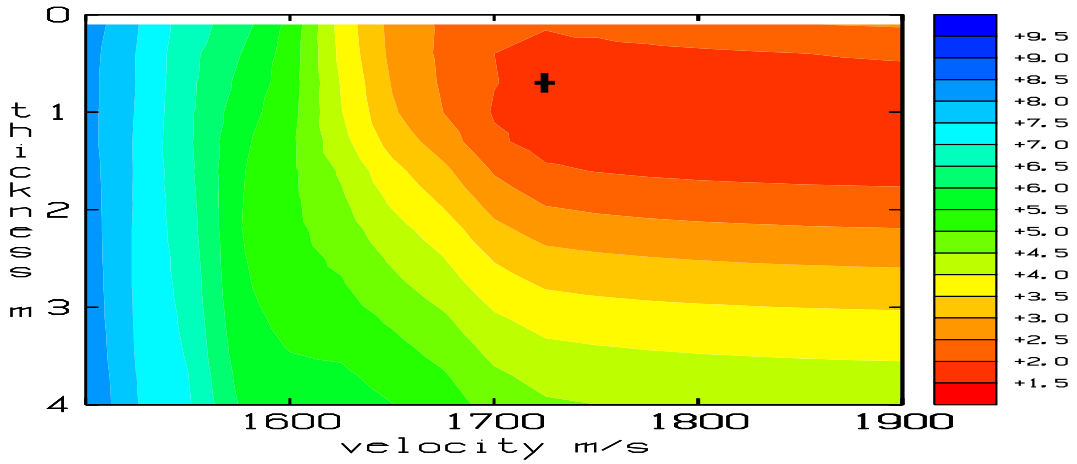

Figure 5.1: *Level plot in dB of the fitness function of the track 1 inversion of 4 kHz data at the source range 250 m, as a function of h_1 and c_{p2}. The peak location of the minimum is marked by a cross.*

It also shows that the velocity of the underlying sediment is certainly larger than some 1600 m/s although the resolution of higher velocities is weak. The ambiguity of the velocity is expected to increase as the thickness of the overlying sediment increases.

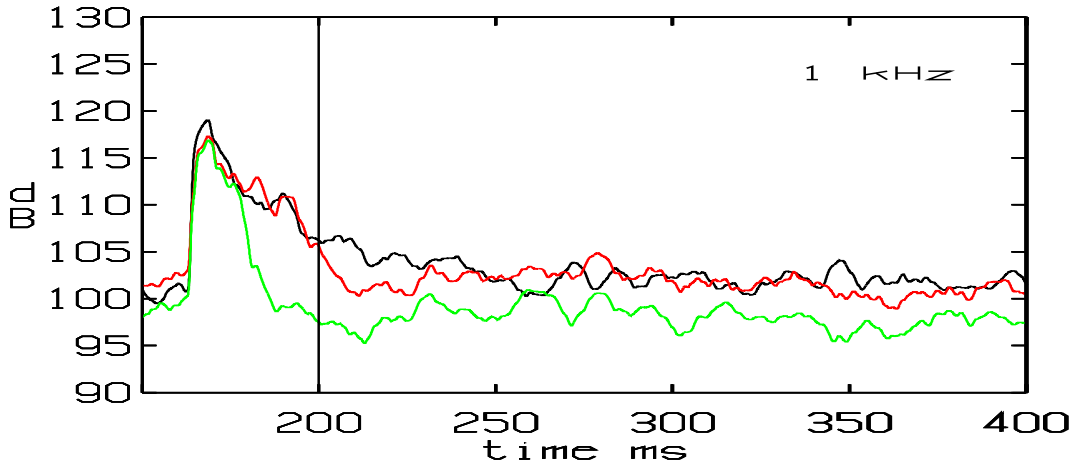

Figure 5.2: *Intensity levels of track 1, propagation range 250 m, 1 kHz field data (black curve) and ray-based simulations (colored curves) for sediment velocities $c_{p2} = 1725$ (red) and $c_{p2} = 1550$ m/s (green). The vertical line marks the right end of the time window for the inversion of 4 kHz data, which resulted in the best fit $h_1 = 0.7$ m and $c_{p2} = 1725$ m/s.*

Figure 5.2 shows model/data comparisons for track 1, range 250 m and 1 kHz. There are two model curves, one with the parameters in Tab. 5.1 (red curve), and another one for which the velocity of the hard sediment was changed to $c_{p2} = 1550$ m/s (green curve). The fitnesses were 1.4 and 7.5 dB, respectively. The modeled time-series is the sum of the fields from two sources at the range 250 m. Besides the transmitted pulse, the field includes the propagation of ship noise at the depth 2 m. We see that the signal computed with a sediment velocity of 1550 m/s is too short. This is explained

by the fact that the critical angle at bottom reflections from the hard sediment are 34° and 23° when the sediment velocities are 1725 and 1550 m/s, respectively. Another observation is that the background level of ship noise drops by some 5 dB for the above decrease of sediment velocity.

Fig. 5.3 illustrates the angular spread of intensity versus time of the computed solution of track 1, source-range 250 m and 1 kHz (red curve in Fig. 5.2). The corresponding plot of acoustic data is shown in Fig. 2.5. In comparing these plots, we note that the extent of the angular spread is about the same but the angular information of the model is more distinct. In the model it is clearly seen that waves travelling at steeper angles arrive later. Another difference is that the modeled noise signal exhibits a notch in the horizontal direction even at the larger range, which is not the case of field data. A possible explanation for this is the omission of bottom scattering of the simplified geoacoustic model being used. The blurred angular content of data may result from a loss of coherence by scattering, which becomes more significant at steeper angles.

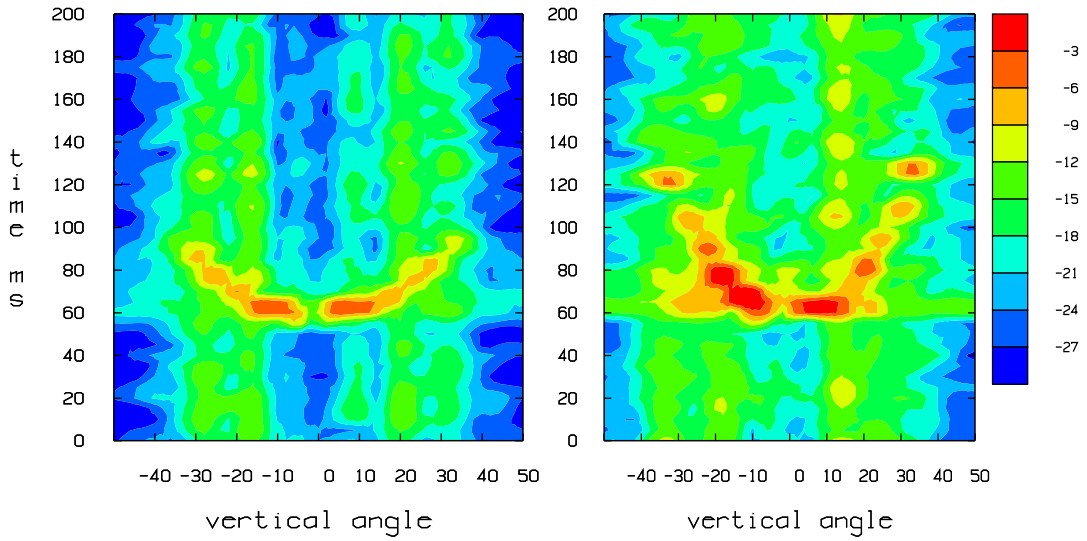

Figure 5.3: *Vertical directionality as a function of time of modeled sound fields of ship noise and a transmitted 1 kHz pulse. The propagation ranges are 250 m (left) and 1 km (right) along track 1. The simulations are based on bottom parameters* $h_1 = 0.7$ *m and* $c_{p2} = 1725$ *m/s of the inversion. The corresponding plot of field data is shown in Fig. 2.5. The intensity levels in these plots are normalized by the peak intensity of field data.*

5.2 The lower sediment

Low frequency data were used for inversion of the thickness and the full set of geoacoustic parameters of the lower sediment, except for the density which was obtained from empirically based regression formulas in terms of the compressional velocity c_{p2}. The sediment was assumed to be homogeneous, and apart from the 1000 m inversion along track 2, the thickness was assumed to be constant as well, cf. Tables 5.3 and 5.4. A genetic algorithm (GA) was used for searching of optimal combinations of the geoacoustic parameters, and the search bounds were for h_2: 2–40 m with resolution 0.6 m, c_{p2}: 1650–1900 m/s (4.0 m/s), c_{s2}: 300–700 m/s (6.3 m/s), β_{p2}: 0.1–1.3 dB/λ (0.04 dB/λ) and β_{s2}: 0.5–2.0 dB/λ (0.05 dB/λ). The thickness of the upper sediment was obtained from the high frequency inversions. The PE-code JEPE-S [22] was used for the forward modeling. This code handles weakly range-dependent fluid-solid media. Inversions were made for 125 Hz and 250 Hz simultaneously at each range, and the results obtained were checked for consistency with 500 Hz data. Tables 5.3 and 5.4 show both inversion results and consistency checks in terms of the fitness function.

	Range 250 m			Range 500 m			Range 1000 m		
frequency [Hz]	**125**	**250**	500	**125**	**250**	500	**125**	**250**	500
fitness [dB]	**2.83**	**2.37**	6.07	**3.96**	**1.68**	4.02	**5.47**	**2.44**	3.83
h_2 [m]	2.60			11.05			2.00		
c_{p2} [m/s]	1753			1880			1880		
c_{s2} [m/s]	605			459			427		
β_{p2} [dB/λ]	1.15			0.41			1.26		
β_{s2} [dB/λ]	2.00			0.55			1.61		

Table 5.3: *Track 1 model/data fitness values of the inversion for the parameters h_2, c_{p2}, c_{s2}, β_{p2}, and β_{s2} respectively of the geoacoustic model (3.1). The inversions were carried out for 125 Hz and 250 Hz simultaneously. The frequency and fitness of the data set selected for inversion are typed in boldface, while the fitness values for 500 Hz were evaluated using the inversion results of those marked by boldface.*

Comparisons with the normal mode model MODELOSS showed discrepancies in the results for the range 250 m, where the seabed is almost flat. While JEPE-S selects a geometry with a thin lower sediment (2-5 m), MODELOSS prefers a thick sediment (20 m). This might be explained by steep angle modes, which give significant contributions to the tail of the signal at this short distance, and which are not accurately represented by a wide angle PE. Accepting the thick sediment result by MODELOSS, we observe a trend towards a thinner lower sediment as the range increases along both tracks. This trend has been used to compile the validation test configuration along track 1 studied in Sec. 5.3, cf. Fig. 5.5.

A common feature of the inversions along both tracks is the problem of matching the relatively fast decay of the 125 Hz data. Increasing the absorptions β_{p2} and/or β_{s2} could result in a better match, but at the expense of wiped out signals at higher frequencies. Another possible loss mechanism might be shear wave resonances for a band of frequencies due to variable thickness of a thin lower sediment. This would affect low frequency signals while leaving high frequency signals almost unaffected.

	Range 250 m			Range 500 m			Range 1000 m		
frequency [Hz]	**125**	**250**	500	**125**	**250**	500	**125**	**250**	500
fitness [dB]	**2.18**	**1.45**	2.88	**5.39**	**3.55**	4.38	**4.83**	**3.83**	5.10
h_2 [m]	5.02			16.48			-		
h_2' [m]	-			-			3.21		
h_2'' [m]	-			-			6.22		
c_{p2} [m/s]	1880			1900			1900		
c_{s2} [m/s]	541			675			687		
β_{p2} [dB/λ]	1.15			0.72			0.10		
β_{s2} [dB/λ]	1.81			1.76			1.13		

Table 5.4: *Track 2 model/data fitness values of the inversion for the parameters h_2, c_{p2}, c_{s2}, β_{p2}, and β_{s2} respectively of the geoacoustic model (3.1). The inversions were carried out for 125 Hz and 250 Hz simultaneously. The media are homogeneous with constant sediment layer thickness, except for the 1000 m inversion where the sediment thickness were allowed to vary: h_2' and h_2'' denote the thickness of the lower sediment at range 500 m and 1000 m respectively, with a linear variation in-between. The frequency and fitness of the data set selected for inversion are typed in boldface, while the fitness values for 500 Hz were evaluated using the inversion results of those marked by boldface.*

As shown in Fig. 2.4, the signal loss for 125 Hz and 250 Hz is larger along track 2 than along track 1. The inversions result in large compressional wave speeds (1880–1900 m/s) along both tracks, while the larger loss along track 2 seems to be accounted for by a larger shear wave speed (675–687 m/s). However, the inversion along track 2 is troublesome, since the signal loss at 125 Hz is considerably larger than for 250 Hz at all ranges. This explains the relatively high fitness values at 500 m and 1000 m in Table 5.4. A similar problem is found in Table 5.3 at 1000 m. According to Fig. 2.4 the 125 Hz signal is weaker than the 250 Hz signal at this range, and the model cannot match the fast decay at 125 Hz. However, the 250 Hz data are well matched, cf. Fig. 5.4. We also observe the importance of the shear wave properties of the lower thin sediment: The green curve shows the modelled time series with the optimal seabed parameters, the red curve the corresponding time series when the shear parameters are cancelled. In the latter case, the model considerably over-estimates the data (black curve). It should be noted that this effect is even higher at 125 Hz.

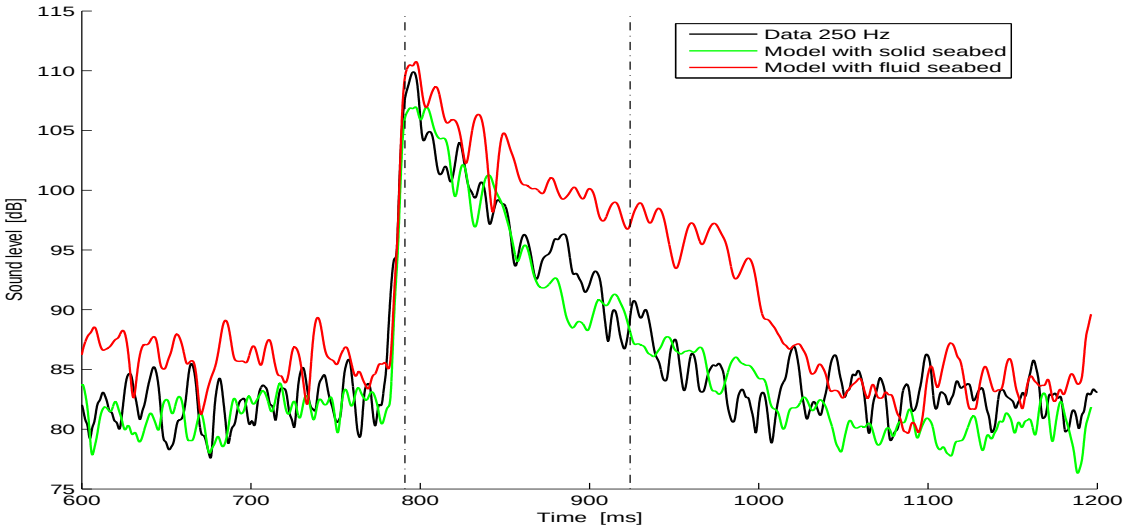

Figure 5.4: Intensity levels of track 1, propagation range 1 km, 250 Hz. The green curve shows the modeled time series with the optimal seabed parameters, the red curve the corresponding time series when the shear parameters are cancelled. In the latter case, the model considerably over-estimates the data (black curve). The vertical lines mark the time window used in the inversion.

5.3 A validation test

In the present experiment, the reception was mixed by noise from the ship that carried the sound projector. As this noise signal was not processed for bottom parameters, it may be used for validation even though it is not an entirely independent measurement. Transmission loss of the ship generated signal was estimated from the recordings and shown in Fig. 2.4. The purpose of the validation test is to compare observed losses with modeled losses using the predicted bottom parameters as input to the sound propagation model. The following geoacoustic model is a compilation of the above inversion results obtained at different frequencies and propagation ranges:

$$\begin{array}{lllllll} \text{layer 1:} & c_{p1}=1400, & \rho_1=1.2, & \beta_{p1}=0.15, & h_1=0.7-3.7 & & \\ \text{layer 2:} & c_{p2}=1880, & c_{s2}=450 & \rho_3=2.08, & \beta_{p2}=0.9, & \beta_{s2}=1.0, & h_2=2-18 \\ \text{layer 3:} & c_{p3}=5200, & c_{s3}=3000, & \rho_3=2.6, & \beta_{p3}=0.2, & \beta_{s3}=0.3 & \end{array} \tag{5.1}$$

The only range-dependent parameters of this model are the sediment thicknesses h_1 and h_2. Fig. 5.5 shows how they vary by range.

In order to appreciate the importance of a proper description of the bottom, simulations were also done for the above geoacoustic model without the top layer. The model/data comparisons are shown in Fig. 5.6.

The differences between measured (black squares) and modeled losses (green squares) based on inversion results are mostly of the same order (< 4 dB) as the fitnesses of the inversions. There are a few large departures. Those at 2 and 4 kHz at 250 and 500 m

are unexpected as the influence of the bottom at these distances is less critical than at 1 and 2 km, where the agreement is good. Trial computations indicated that the uncertainty of the assumed depth of the noise source at 2 m could be a contributing factor. Another one is the assumed steadiness of the actual noise source.

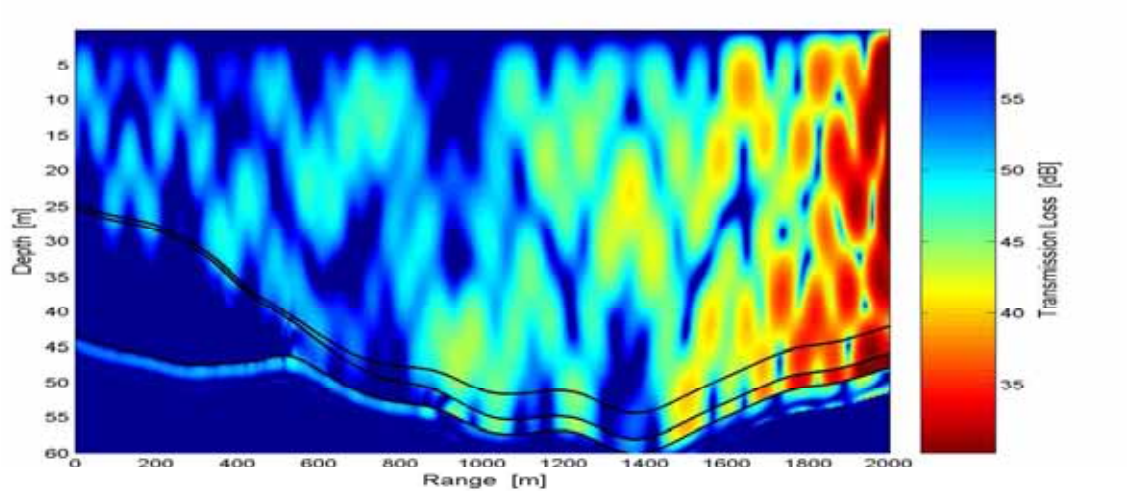

(a) 125 Hz

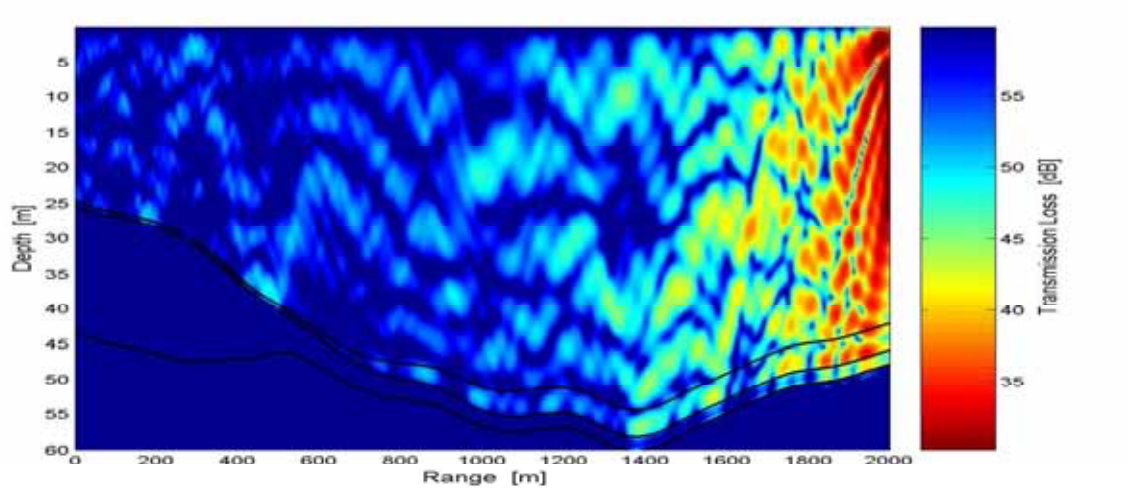

(b) 500 Hz

Figure 5.5: Transmission loss computed by JEPE-S for the validation test environment (5.1). The larger penetration depth at the lower frequency is discernable.

The red squares represent losses over a hard sediment without a soft cover. It is clear that predictions based on such a bottom would underestimate the losses by more than 10 dB at a range of 2 km and at frequencies larger than 500 Hz. Even though the bottom description of the inversion is coarse, this test indicates that it captures the main characteristics that is needed for making reasonable predictions of sound propagation.

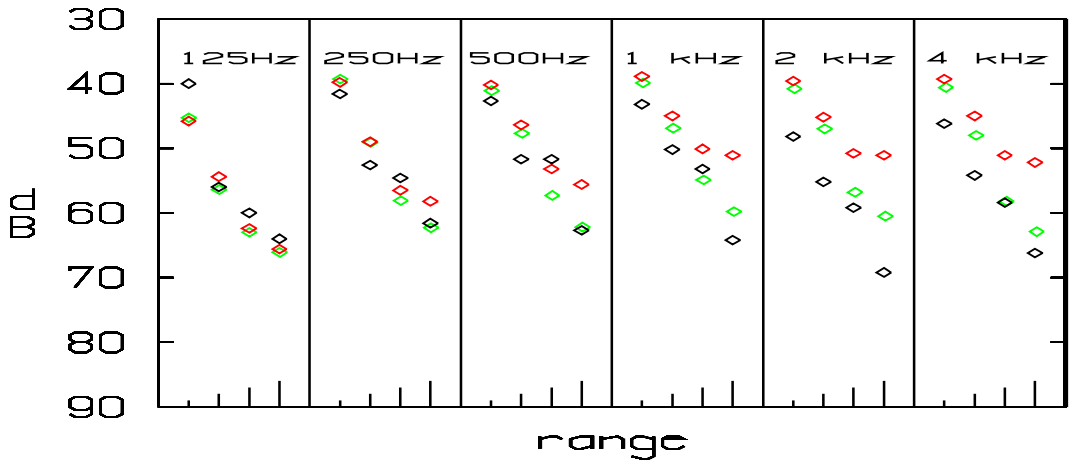

Figure 5.6: *Transmission loss at propagation ranges of 0.25, 0.5, 1, and 2 km along track 1. These ranges are represented by tick marks of increasing lengths at the bottom of each frequency panel. Black squares denote the measured ship noise from HMS Ägir. Simulated losses for an geoacoustic model based on inversion results are marked by green squares. Those in red squares are predictions made by the same model without the top layer.*

6 Summary

6.1 TL versus RL inversions

This report concludes the geoacoustic analysis of data from the field trial in June 2005. Two types of data sets were collected , transmission loss (TL) and reflection loss (RL) data. The analysis of RL data were reported in [1]. The sound source, the transmitted wave forms, the receiver array, and the test site were the same. Apart from that the characteristics of data and the inversion techniques are different. RL data were collected at source-receiver ranges between 25 and 100 m, while TL data were obtained at the propagation distances between 0.25 and 4 km. RL data consist of a set of reflection coefficients as function of grazing angle of bottom reflected waves. The vertical source-receiver geometry was exploited to extract a bottom echo of the signal at each hydrophone. TL data consist of received energy, averaged over all hydrophones, as a function of time. In the RL case, the bottom parameters were determined by matching measured and computed losses using the conventional Rayleigh model of plane wave reflections at the bottom. Due to the simplicity of this approach, the inversions could be effectuated within a run time of a second. TL data embody a more comprehensive response of the acoustic environment including effects of bathymetry, sound refraction and sea surface, bottom and subbottom reflections. The computational cost of disentangling these effects by the matched-field technique varies widely depending on propagation distance, topography, and bandwidth of probing signals.

The TL inversions at the shortest source-receiver range 250 m is of particular interest as there is a fair overlap with the propagation ranges 25–100 m of the RL measurements at the same site. For a shared geoacoustic model with a low-speed layer on top of a sediment with shear rigidity the following inversion results were obtained for the

thickness (h_1) of the top layer and the compressional velocity (c_{p2}) of the underlying sediment:

TL data 4 kHz :	$h_1 : 0.7$ m,	$c_{p2} : 1725$ m/s
RL data 4 kHz :	$h_1 : 0.1 - 0.4$ m,	$c_{p2} : 1575 - 1757$ m/s

The RL inversions were performed in various directions around the array. It was found that the bottom parameters exhibited lateral variations on a scale of only a few tens of metres, which explains the interval estimates of the RL inversion. Both results show that the seafloor is quite hard. In view of the simplified geoacoustic model, the thickness of the top layer is so thin that it might be interpreted as a softening of the surface of the hard sediment by irregular embeddings of clay.

6.2 Future directions

Only mobile data acquisition systems can provide the operational speed needed for accurate bottom mappings of large areas. To accomplish this, the response time of inversions must be comparable with the time for data collection. Several keys of solving this difficulty have been gained from the present and past geoacoustic experiments. One is that inversions of reflection data can be performed within a second of computer time. The above RL approach is the simplest one. Its capability is limited to predictions of the velocity of the surficial sediment and possibly the thickness of a soft layer. A more elaborate approach is to capture subbottom echoes and to infer sediment velocities and thicknesses by travel time analysis, while density and absorption parameters are determined by echo amplitudes. Such an extension is similar to the well-known wide-angle reflection method in seismology. It allows inversions in real time by matching of arrival times and amplitudes using ray-based modeling [12, 13]. The main difficulty is to assure a source-receiver geometry so that bottom and subbottom echoes can be isolated from the direct arrival and the sea surface reflection. In shallow water, good time resolution is also necessary, although decreased bottom penetration at higher frequencies is a trade off. These difficulties can largely be dispensed with at the expense of increasing the model complexity like the TL approach of the present paper. This technique requires just one source-receiver pair with a separation distance of a few hundred meters. The demand on positional accuracy of the sonar system is much less than for reflection analysis. Signals in both low and high frequency bands should be used for surveying at varying subbottom depths. The use of own ship noise for inversion is a noteworthy possibility. The main difficulty is the high computational cost of full-field modeling. A segmented approach in range is a definite prerequisite so that range-independent modeling applies within the range window of the source receiver offset. In addition, inversion schemes based on incremental updates of bottom parameters need to be developed as to avoid full inversions from ground floor. It is envisaged that range-independent inversions based on ray (high frequency data) and normal-mode (low frequency data) modelling could be completed within minutes. It appears that the TL approach is to be preferred in open waters, where a large aperture is easier to realize, and the condition of range-independence over some hundreds of metres is more likely to be satisfied.

Acknowledgement

We thank CO Jonni Tvinghagen and the crew of HMS Ägir for their assistance in seagoing operations.

We also like to thank Per Morén for his constructive participation at several stages of this work.

References

[1] L. Abrahamsson, B.L. Andersson, E. Dalberg, S. Ban, and P. Söderberg. Geoacoustic inversion of reflection loss data. Technical report FOI-R–1726–SE, 2005.

[2] B.G. Katsnelson and V.G. Petnikov. *Shallow-Water Acoustics*. Springer, Praxis, 2002.

[3] J. Pihl, J.-O. Hegethorn, S. Ivansson, P. Morén, E. Norrbrand, B. Nilsson, G. Sundin, A. Wester, and V. Westerlin. Underwater Acoustics in the Baltic. Technical report FOA-R-97-00727-409–SE, 1998.

[4] L. Berghult and A. Wester. TRANSMISSION LOSS MEASUREMENTS IN THE ARCHIPELAGO (MÄLSTEN AND GUSTAF DAHLÉN). In *HYDROAKUSTIK 1995*. FOA-R–95-00173-2.2–SE, 1995.

[5] O.F. Hastrup. Some bottom-reflection loss anomalies near grazing and their effect on propagation in shallow water. In *Bottom-Interacting Ocean Acoustics, ed. W.A Kuperman and F.B. Jensen*, pages 135–152, New York, 1980.

[6] L.A. Rubano. Acoustic propagation in shallow water over a low-velocity bottom. *J. Acoust. Soc. Amer.*, 67:1608–1613, 1980.

[7] C.W. Holland. Geoacoustic inversion for fine-grained sediments. *J. Acoust. Soc. Amer.*, 111:1560–1564, 2002.

[8] G.M. Bryan. The hydrophone-pinger experiment. *J. Acoust. Soc. Amer.*, 68:1403–1408, 1980.

[9] E.L. Hamilton. Refection coefficients and bottom losses at normal incidence computed from pacific sediment properties. *Geophysics*, 55:995–1004, 1970.

[10] O.F. Hastrup. Digital Analysis of Acoustic Reflectivity in the Tyrrhenian Abyssal Plain. *J. Acoust. Soc. Amer.*, 47:181–190, 1969.

[11] R.S. Winokur and J.C. Bohn. Sound Reflection from a Low-Velocity Bottom. *J. Acoust. Soc. Amer.*, 44:1130–1138, 1968.

[12] L. Abrahamsson, E. Dalberg, T. Fristedt, and P. Sigray. Measurements and analysis of sound reflected from the seabed. Technical report FOI-R–1689–SE, 2004.

[13] L. Abrahamsson, B.L. Andersson, I. Karasalo, and P. Sigray. Environment assessment for underwater sensors in the Stockholm archipelago, Part 1 - Inversion of hydroacoustic sub-bottom parameters. User report FOI-R–0706–SE, 2002.

[14] J.-P. Hermand. Broad-Band Geoacoustic Inversion in Shallow Water from Waveguide Impulse Response Measurements on a Single Hydrophone: Theory and Experimental Results. *IEEE J. Oceanic Eng.*, 24:41–66, 1999.

[15] F.B. Jensen. Sound propagation in shallow water: A detailed description of the acoustic field close to surface and bottom. *J. Acoust. Soc. Amer.*, 70:1397–1406, 1981.

[16] B.E. Tucholke. Acoustic environment of the Hatteras and Nares Abyssal Plains, western North Atlantic Ocean, determined from velocities and physical properties of sediment cores. *J. Acoust. Soc. Amer.*, 68:1376–1390, 1980.

[17] A.L. Anderson and L.D. Hampton. Acoustics of gas-bearing sediments I. Background. *J. Acoust. Soc. Amer.*, 67:1865–1889, 1980.

[18] J. Pihl and L. Abrahamsson. MODELOSS - A User Oriented Code for Transmission Loss Calculations. FOA report R-95-00173-2.2-SE, 1995.

[19] R.T. Bachman. Acoustic and physical property relationships in marine sediments. *J. Acoust. Soc. Amer.*, 78:616–621, 1985.

[20] E.L. Hamilton. Compressional-wave attenuation in marine sediments. *Geophysics*, 37:620–646, 1972.

[21] A.I. Eller and D.A. Gershfeld. Low-frequency acoustic response of shallow water ducts. *J. Acoust. Soc. Amer.*, 78:622–631, 1985.

[22] B.L. Andersson. JEPE-S, a PE code for wave propagation in range-dependent fluid-solid media. Technical report FOA-R–98-00979-409–SE, 1998.

[23] L. Abrahamsson. RAYLAB - a ray tracing program in underwater acoustics. Scientific report FOI-R–1047–SE, 2003.